Journal of Zhejiang University-SCIENCE A (Applied Physics & Engineering)
ISSN 1673-565X (Print); ISSN 1862-1775 (Online)
www.jzus.zju.edu.cn; www.springerlink.com
E-mail: jzus@zju.edu.cn

Numerical simulation of partial-interaction load-deflection behavior of corroded reinforced concrete beams based on a segmental approach and evaluation of reinforcement corrosion level*

Qian FENG[1], Guan-nan WANG[1], Yong-ping ZHANG[2], Rong-qiao XU[†‡1]

[1]*College of Civil Engineering and Architecture, Zhejiang University, Hangzhou 310058, China*

[2]*School of Mechanics and Engineering Science, Shanghai University, Shanghai 200444, China*

[†]E-mail: xurongqiao@zju.edu.cn

Received Dec. 4, 2019; Revision accepted Mar. 23, 2020; Crosschecked Mar. 31, 2020

Abstract: Corrosion of reinforcement has a significant effect on the deformation of reinforced concrete beams by deteriorating the bond-slip characteristics, diminishing the cross-sectional area of reinforcement, and causing cracking. The traditional way of quantifying the load capacity and simulating deflection is the moment-curvature (M/χ) approach. The problem is that the M/χ approach is semi-empirical after cracking as it is strain-based and cannot allow for tension stiffening. This paper introduces the new displacement-based moment-rotation (M/θ) approach which directly simulates the development of cracks and hence allows for tension stiffening. This M/θ approach is then used to predict the load-deflection behavior of reinforced concrete beams with corrosion effect by incorporating the corrosion-affected bond-slip model. The bond-slip model only considers the corrosion effect but ignores the confinement effect. It is used here as an example to describe the procedure of how to quantify the corrosion effect on reinforced concrete beam behavior. The load-deflection curves obtained from the numerical simulation show a good agreement with test results. For reinforced concrete beams with confinement, the only difference is to replace the bond-slip model with the one which includes both corrosion and stirrup effects. Additionally, the paper shows how to use the M/θ approach with the bond-slip model to predict the real corrosion level of reinforcement in some tests in which only the theoretical corrosion levels are provided.

Key words: Reinforced concrete; Corrosion; Partial interaction; Load-deflection; Tension-stiffening; Bond-slip
https://doi.org/10.1631/jzus.A1900616 **CLC number:** U441.2

1 Introduction

Corrosion of reinforcement in concrete beams leads to cracking, deterioration of the bond-slip relationship, and reduction of steel cross-section (Al-Sulaimani et al., 1990; Almusallam et al., 1996a; Cabrera, 1996; Lee et al., 2002; Fang et al., 2004). These cause the loss of load capacity and increase of deflection (Almusallam et al., 1996b; Mangat and Elgarf, 1999; Jin and Zhao, 2001; Dekoster et al., 2003; Feng et al., 2018; Jiang et al., 2018). The deterioration of bond-slip characteristics caused by steel corrosion enlarges crack widths, influences crack spacing, and weakens the flexural rigidity, and will finally affect the flexural behavior of reinforced concrete (Knight et al., 2013, 2014; Jiang et al., 2018; Visintin et al., 2018).

As a traditional way of simulating the behavior of reinforced concrete members, the moment-curvature (M/χ) approach is used to quantify the flexural rigidities by incorporating the principle of plane

‡ Corresponding author
* Project supported by the National Natural Science Foundation of China (No. 51478422)
ORCID: Qian FENG, https://orcid.org/0000-0002-5152-8599; Rong-qiao XU, https://orcid.org/0000-0002-0005-9737

sections remaining plane after bending and the linear strain profile (Branson, 1977; Thompson and Park, 1980; Gilbert and Mickleborough, 1990; Warner et al., 1998; Nawy, 2006). It is strain-based and mechanically correct prior to the cracking of the tensile concrete since the material stress-strain relationship is the only empirically derived component (Knight et al., 2013, 2014; Visintin et al., 2013a, 2013b). However, after cracking, the M/χ approach adopts an effective flexural rigidity to simulate tension stiffening instead of considering slip between reinforcement and adjacent concrete. This means that the M/χ approach cannot simulate the mechanics of tension stiffening.

To overcome this problem, the moment-rotation (M/θ) approach was developed to allow for tension-stiffening effects in members which were reinforced with either steel or fiber-reinforced polymer (FRP) (Oehlers et al., 2011; Visintin et al., 2012, 2013a, 2013b; Knight et al., 2013, 2014, 2015). It gives exactly the same results as the M/χ approach prior to cracking (Knight et al., 2013, 2014). After cracking, however, the displacement-based M/θ approach has an advantage since it allows for crack of concrete and slip between concrete and reinforcement. By applying the mechanics of partial-interaction theory (Oehlers et al., 2005, 2011, 2013; Haskett et al., 2008, 2009; Muhamad et al., 2011, 2012; Knight et al., 2015) in the M/θ approach, it directly simulates the tension-stiffening effects by incorporating the development of cracks and the slip between reinforcement and the adjacent concrete.

The M/θ approach is extended in this study to investigate corroded reinforced concrete beams. By changing the material properties and incorporating bond-slip characteristics caused by corrosion (Al-Sulaimani et al., 1990; Almusallam et al., 1996a; Yalciner et al., 2012; Feng et al., 2016; Jiang et al., 2018; Lin et al., 2019), the displacement-based M/θ approach simulates the flexural behavior of reinforced concrete beams changing with corrosion levels of reinforcement. Having been applied to allow for corroded reinforcement, the M/θ approach is then extended to predict the instantaneous deflections of reinforced concrete members with those tested by Lee et al. (1998) and Mangat and Elgarf (1999). A good correlation between theoretical results and test results is observed.

This study is focused on the short-term flexural behavior of reinforced concrete beams and hence the time effects such as creep and shrinkage are not considered here. However, these could also be allowed for in the M/θ approach (Visintin et al., 2013b). The flexural behavior of the reinforced concrete without stirrup effects is discussed here. Also the work could, in a further step, be extended to the analysis of load-deflection responses of reinforced concrete with confinement effects by changing the bond-slip characteristics.

2 Bond-slip characteristics of corroded reinforced concrete beams without confinement

2.1 Relationship between k_τ and corrosion level

Many previous studies demonstrate that the change of bond strength with corrosion level should be divided into three stages as exhibited in Fig. 1. The abscissa is the corrosion level of reinforcement normally measured as percent mass loss of the original reinforcement. The ordinate is k_τ which represents the bond strength $\tau_{\max}$ deteriorated by corrosion normalized by the bond strength of non-corroded reinforcement. Hence, the bond strength due to corrosion could be calculated by

$$\tau_{\max} = k_\tau \tau_{\max 0}, \tag{1}$$

where $\tau_{\max 0}$ is the bond strength for non-corroded reinforcement.

At the first stage marked as 'Stage 1' in Fig. 1, when corrosion increases, the bond strength between reinforcement and adjacent concrete slightly increases. The bond strength peaks at point A where the corrosion level is equal to $\mathrm{cor}_{\mathrm{pk}}$. Then the bond strength decreases to the value of $\tau_{\max 0}$ at point B where the corrosion level is equal to $\mathrm{cor}_{1\text{-}2}$. During this stage, the bond strength influenced by corrosion is always slightly larger than the bond strength of non-corroded reinforcement. However, for reasons of design or safety k_τ is suggested to be taken as 1 in Stage 1 which goes directly from point O to point B (Feng et al., 2016, 2018).

The second stage from point B to point C in Fig. 1 is where the bond strength drops dramatically as the corrosion level continues to increase from $\mathrm{cor}_{1\text{-}2}$ to $\mathrm{cor}_{2\text{-}3}$. During this stage, the relationship between bond strength and corrosion level (cor) could be depicted by

$$k_\tau = k_{\tau\text{-k}}\text{cor} + k_{\tau\text{-b}}, \quad (2)$$

where $k_{\tau\text{-k}}$ is the slope of the linear descending branch, and $k_{\tau\text{-b}}$ is the intercept.

The third stage starting from point *C* in Fig. 1 is when the residual bond strength remains at almost a constant value even when the corrosion level continues to grow beyond $\text{cor}_{2\text{-}3}$.

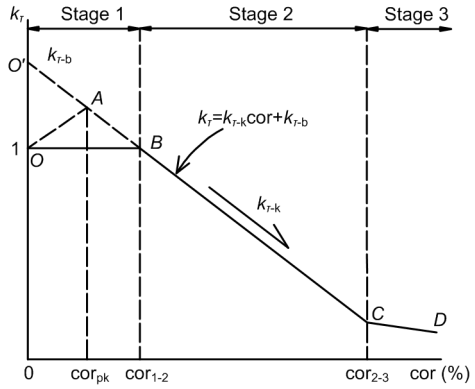

Fig. 1 Relationship between k_τ and corrosion levels

2.2 Bond-slip relationship changing with corrosion

The FIB model code (FIB, 2013) suggests that the local bond-slip (τ-δ) relationship without stirrup confinement usually includes two parts: the non-linear ascending branch and the linear descending branch shown as *O*-*A*-*B* in Fig. 2. The slip δ_1 corresponds to the bond strength $\tau_{\max0}$ which represents the slip value when the bond stress reaches the peak value. Meanwhile, $\delta_{\max}$ is the slip value when the bond stress in the descending branch decreases to zero. As explained in Section 2.1, the bond strength values are $\tau_{\max0}$ for corrosion levels ranging from 0 to $\text{cor}_{1\text{-}2}$. Hence, during this stage, the bond-slip responses are the same as *O*-*A*-*B* in Fig. 2.

As the corrosion level continues to rise, the bond strength deteriorates rapidly. Several varying bond-slip responses due to different corrosion levels are exhibited in Fig. 2. As the corrosion level increases from $\text{cor}_{1\text{-}2}$ to $\text{cor}_{2\text{-}3}$, the bond strength value drops from $\tau_{\max0}$ to $\tau_{\max3}$. The shape of the bond-slip relationship is *O*-*C*-*D* in Fig. 2 for a corrosion level equal to $\text{cor}_{2\text{-}3}$.

For corrosion levels larger than $\text{cor}_{2\text{-}3}$, bond strength may decline slightly as shown in the k_τ-cor relationship in Fig. 1, in which case the bond strength may decrease to $\tau_{\max4}$ in Fig. 2 and the corresponding bond-slip shape is depicted as *O*-*E*-*F*.

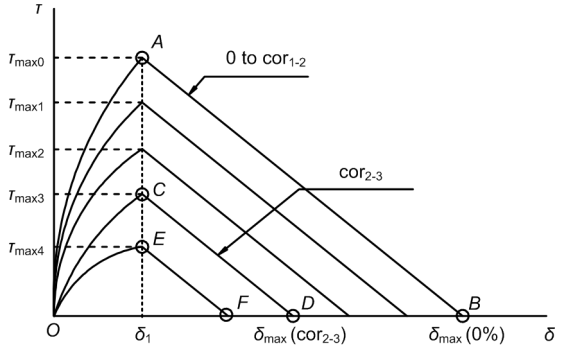

Fig. 2 Bond-slip responses due to different corrosion levels

3 Moment-rotation approach prior to crack

A segment of a corroded reinforced concrete member is depicted in Fig. 3 with the cross-section of the segment described in Fig. 3a and the lengthwise view in Fig. 3b. There are tensile and compressive reinforcements embedded in the concrete. The segment is symmetrical in dimension about the datum C-C and is also symmetrically loaded as shown in Fig. 3a. The ends of the concrete component of the segment are represented by lines A-A. The length of the segment $2L_{\text{def}}$ is equal to the crack spacing with half of the length equal to L_{def}. Now a constant moment *M* is applied over the segment causing the deformation of the concrete component from lines A-A to B-B based on the principle of plane section remaining plane. The total rotation as shown in Fig. 3b is θ.

By symmetry, it is only necessary to consider half of the segment of length L_{def}. In this case, the right half of the segment is taken to simulate segment behavior prior to cracking as shown in Fig. 4. The deformation of the concrete component is from lines A-A to B-B as shown in Fig. 4a. The deformation of tensile reinforcement is Δ_{rt}, and the deformation of compressive reinforcement is Δ_{rc}. Fig. 4b depicts the deformations caused by rotation θ. Fig. 4c depicts the linear strain profile which is the deformation in Fig. 4b divided by the length L_{def}. The curvature χ is equal to θ/L_{def}. Then the strains induce stresses as shown in Fig. 4d based on the material stress-strain relationships

for concrete and reinforcement. Fig. 4e gives the distribution of forces by the integration of the stress profiles in Fig. 4d.

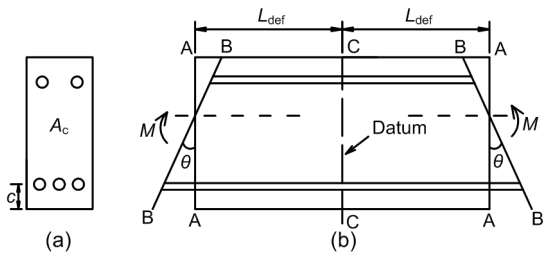

Fig. 3 Deformation of the segment

(a) Cross-section; (b) Beam segment. A_c is the cross-sectional area; c is the concrete cover of reinforcement

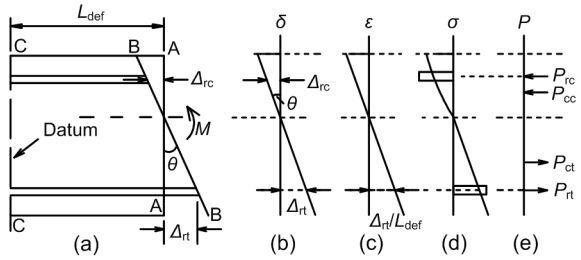

Fig. 4 Segmental analysis prior to cracking

(a) Beam segment; (b) Deformation; (c) Strain ε; (d) Stress σ; (e) Force P. P_{rc} and P_{cc} are the compressive forces on reinforcement and concrete, respectively; P_{rt} and P_{ct} are the tensile forces on reinforcement and concrete, respectively

At the stage when the cracking has not yet started, the stress profile is obtained directly from the strain profile for the provided material stress-strain relationships. To find a solution to the analysis in Fig. 4, an iterative approach can be used here by the following steps:

1. For a fixed θ, guess a neutral axis depth value d_n, based on which the deformations shown in Fig. 4b could be determined.

2. The strain profile in Fig. 4c is obtained by dividing the deformation by L_{def}.

3. The stress profile in Fig. 4d is then determined from the strain profile in Fig. 4c based on the given material stress-strain relationships.

4. The internal forces in Fig. 4e are determined by the integration of the stresses along the stress profile in Fig. 4d.

5. Check whether the algebraic sum of these forces is equal to zero. If it is, go to the next step. Otherwise, shift the depth of the neutral axis and repeat steps 1–4 until the internal forces sum to zero.

6. The moment value is determined for a specific θ.

7. By increasing the rotation value and repeating steps 1–6, the moment-rotation relationship can be derived.

As mentioned above, the derived moment-rotation relationship can be changed into a moment-curvature relationship by dividing the rotations by the length L_{def}. At the uncracked stage, the stress profile is determined directly from the strain profile with material stress-strain relationships, which means it is the strain-based analysis. Hence, the results from the M/θ approach and those from the M/χ approach are exactly the same. That is because both approaches are full-interaction (FI) analysis.

4 Moment-rotation approach after cracking

4.1 Moment-rotation approach

After cracking, the M/χ analysis assumes that there is no interaction between tensile reinforcement and the adjacent concrete. However, in reality, when the crack tip crosses the reinforcement, there is slip between reinforcement and concrete which requires the partial interaction analysis to allow for tension stiffening.

At the stage of cracking, it is shown in Fig. 5 that the applied load on the segment, in Fig. 5a, causes the deformation and the rotation θ in Fig. 5b. Then the deformation gives the strain profile in Fig. 5c. In the compressive region, the compressive stresses of both concrete and reinforcement in Fig. 5d are determined based on the strain profile in the compressive region in Fig. 5c as this is still FI analysis. The tensile stresses of concrete in the tensile region are also obtained directly from the strain profile as long as the corresponding strain value is no larger than the concrete tensile capacity ε_{ct}. However, the stress of tension reinforcement in Fig. 5d is not obtained directly from the strain profile. The partial-interaction theory must be introduced to allow for tension stiffening.

To simulate tension stiffening, a concentrically loaded reinforced concrete prism was taken from the segment as shown in Fig. 5a to do the analysis. This is common practice both experimentally and theoretically

(Haskett et al., 2008; Visintin et al., 2013b). The prism taken from the segment between two crack faces is shown in Fig. 6 with the cross-section in Fig. 6a and the lengthwise view in Fig. 6b. Both the covers on top of the reinforcement and under the reinforcement are c symmetrically. The cross-sectional area of the prism is A_c. The sum of the cross-sectional area of reinforcing bars is A_r. The perimeter length between reinforcing bars and concrete is L_{per}. It is shown in Fig. 6b that in the numerical simulation of tension stiffening, the prism was sliced into a large number of very short elements so that the slip Δ within an element is assumed to be constant (Haskett et al., 2008; Oehlers et al., 2011). The length of each element is L_s.

It is shown in Fig. 6b that if the crack width is $2\Delta_{rt}$, then the numerical simulation gives the value of the corresponding force on reinforcement P_{rt}. It means that based on the deformation provided by Fig. 5b, the internal force on reinforcement could be obtained to check whether the sum of the internal forces on reinforcement and concrete has reached equilibrium or not. Hence, at the stage of cracking, the issue can therefore be summarized as: (1) simulating the mechanism of tension stiffening, (2) locating the crack to predict the length of the segment, and (3) determining the internal force on reinforcement for a certain slip. A well-established numerical technique (Oehlers et al., 2005, 2011, 2013; Haskett et al., 2008, 2009; Muhamad et al., 2011) is introduced here to be adapted for the M/θ analysis.

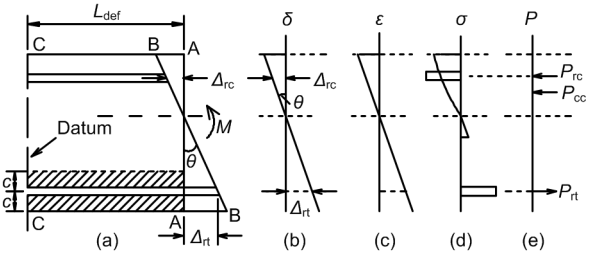

Fig. 5 Segmental analysis after cracking

(a) Beam segment; (b) Deformation; (c) Strain; (d) Stress; (e) Force

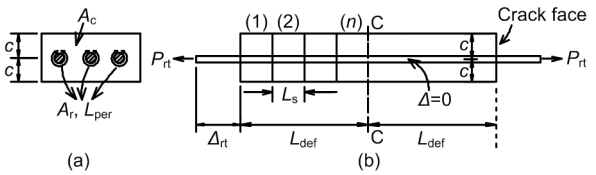

Fig. 6 Tension-stiffening analysis

(a) Prism cross-section; (b) Lengthwise view of prism

4.2 Tension stiffening analysis

The interaction between reinforcement and concrete is described by taking two adjacent elements from the prism as an example to illustrate the tension stiffening mechanism. This is shown in Fig. 7. Element 1 in Fig. 7a is the one with the crack face on the left hand side, which means that Δ_1 is also the slip Δ_{rt} between reinforcement and concrete at the crack face. The force on reinforcement P_1 is P_{rt} at the crack face while the force C on concrete at the crack face is zero. By assuming the slip is constant along the length L_s within an element, the bond stress τ is therefore constant within an element which gives the bond force B_1 as

$$B_1 = \tau_1 L_{per} L_s. \tag{3}$$

Hence, the force on concrete on the right-hand side of element 1 increases to B_1 while the force on reinforcement on the right-hand side of element 1 decreases to $P_{rt}-B_1$. Based on the material properties, the mean strain of reinforcement ε_{r1} in element 1 can be expressed by

$$\varepsilon_{r1} = \frac{2P_{rt} - B_1}{2E_r A_r}, \tag{4}$$

where E_r is the elasticity modulus of reinforcement, and A_r is the cross-sectional area of reinforcement. The mean strains of concrete ε_{c1} in element 1 can be expressed by

$$\varepsilon_{c1} = \frac{0 + B_1}{2E_c A_c}, \tag{5}$$

where E_c is the elasticity modulus of concrete.

The slip-strain $d\Delta_1/dx$, which represents the strain difference in element 1, can be described by

$$\frac{d\Delta_1}{dx} = \varepsilon_{r1} - \varepsilon_{c1}. \tag{6}$$

Hence, the change of slip in element 1 can be determined by

$$\delta\Delta_1=(\varepsilon_{r1}-\varepsilon_{c1})L_s. \quad (7)$$

Similarly, the change of internal force, the bond stress, the strains, and slip of element 2 can be deduced in the same way, which is shown in Fig. 7. Consequently, by repeating the procedure along the length of the prism, the parameters in element n can be determined. The bond force B_n is equal to $\tau_n L_s L_{per}$, in which τ_n is derived from Δ_n based on the bond-slip model. The force in the concrete on the right side of element n is P_{cn}, equal to $P_{c(n-1)}+B_n$. The force in the reinforcement on the right side of element n is P_{rtn} equal to $P_{rt(n-1)}-B_n$. The concrete strain ε_{cn} along element n is $(P_{c(n-1)}+P_{cn})/(2E_cA_c)$. The strain of reinforcement ε_{rn} is $(P_{rt(n-1)}+P_{rtn})/(2E_rA_r)$. The value of the difference of strain between concrete and reinforcement $d\Delta_n/dx$ is $\varepsilon_{rn}-\varepsilon_{cn}$. The change of slip $\delta\Delta_n$ in element n is $(\varepsilon_{rn}-\varepsilon_{cn})L_s$. Consequently, the slip Δ_{n+1} on the right side of element n can be obtained as $\Delta_n-\delta\Delta_n$. This is an iterative solution by guessing the internal force on reinforcement P_{rt} at the crack face for the required slip value and applying the boundary condition into the method to check whether the evaluated value of P_{rt} is correct.

Normally, the boundary conditions are not the same for different cases. For example, in short prisms in which the reinforcement is anchored, the boundary condition would be that the slip between reinforcement and concrete is zero at the position of anchorage. For the short prisms in which the reinforcement is not anchored, the boundary condition of ε_r equal to zero at the end of reinforcement may be applied in the analysis.

In the long prisms in Fig. 8a, where PI indicates partial-interaction, the boundary condition for reaching the FI point would be somewhere along the length of the prism. Both slip Δ in Fig. 8b and slip-strain $d\Delta/dx$ in Fig. 8c are zero or tend to zero at the same location. In this case, the tension stiffening analysis can be used to decide the primary crack spacing S_{cr}.

Once a crack has formed at the length of S_{cr}, the analysis is referred to as multiple-crack analysis to get the load for certain slip values at the crack face. The prism in Fig. 9a is symmetrically loaded. The boundary condition is that the slip Δ between reinforcement and concrete is equal to zero mid-way along the prism as shown in Fig. 9b.

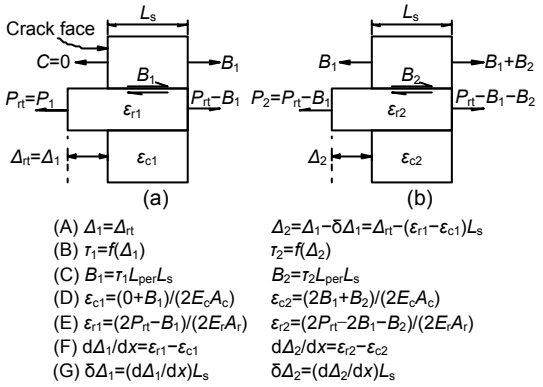

Fig. 7 Iterative approach of tension stiffening
(a) Element 1; (b) Element 2

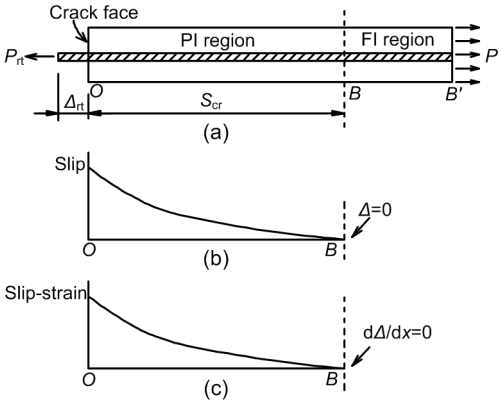

Fig. 8 Single crack analysis
(a) Prism; (b) Slip distribution; (c) Slip-stain distribution

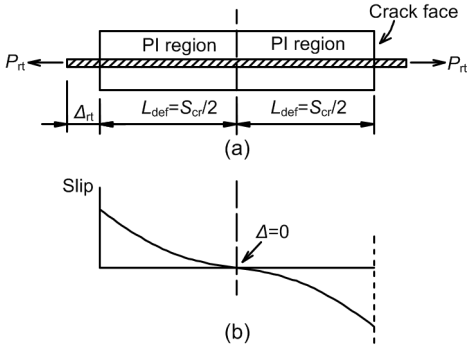

Fig. 9 Multiple-crack analysis
(a) Prism; (b) Slip distribution

5 Procedure to get deflection

The deflection distribution along the beam for certain loads can be determined by using techniques of standard analysis. For example, the simply supported

beam in Fig. 10 is under a four-point bending test as shown in Fig. 10a. The moment distribution is developed as depicted in Fig. 10b because of the application of the transverse load P. From the derived M/θ relationship, the rotation distribution along the beam can also be obtained based on the varying moment values along the beam. Then, derived by dividing the rotation by the prism length, the curvature distribution along the beam is shown in Fig. 10c. The curvature values along the beam can then be integrated twice to determine the deflection of the beam by standard analytical techniques. Finally, for different load values, the corresponding mid-deflection values can be obtained by repeating the above steps. This gives the load-deflection curve.

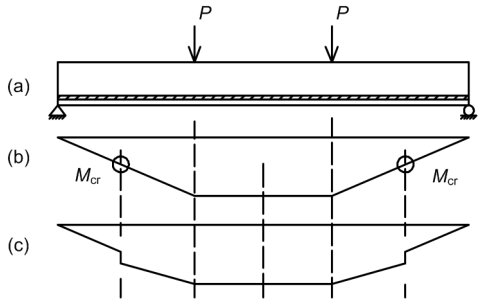

Fig. 10 Deflection distribution by standard analytical techniques: (a) beam; (b) moment; (c) curvature (M_{cr} means the moment causing crack)

6 Application to results from corrosion tests

The material model of bond-slip changed with corrosion in Section 2 and the segmental M/θ approach described in Sections 3 and 4 are used to determine the load-deflection responses of corroded reinforced concrete beams tested by Lee et al. (1998). This has been compared with the finite element analysis carried out by Dekoster et al. (2003). The fitting of load-deflection responses is shown in Section 6.2. Then, the M/θ approach and the bond-slip model are adopted in Section 6.3 for two purposes. One is to compare the results from the proposed numerical approach with the test results of 0% corrosion level. The other is to determine the corrosion levels of those test samples for which the real corrosion levels measured as mass loss were not given in this paper.

Normally, researchers measured the real corrosion levels after the test through the extraction and cleaning of the reinforcement (Al-Sulaimani et al., 1990; Almusallam et al., 1996a; Jin and Zhao, 2001; Fang et al., 2004, 2006). However, this step was sometimes skipped by researchers and only theoretical corrosion levels were given in the literature (Mangat and Elgarf, 1999; Tondolo, 2015). Also, many tests provided corrosion degrees of reinforcement using different calculation methods (Johnston and Cox, 1940; Peattie and Pope, 1956; Chapman and Shah, 1987; Fu and Chung, 1997; Lundgren, 2002) such as diameter loss or exposure time of test samples. The provided theoretical corrosion levels in the literature (Mangat and Elgarf, 1999) were not defined as percent mass loss of reinforcement but the values offer important information for determining the real corrosion levels for the reinforcement. The procedure for predicting the real corrosion level as percent mass loss based on load-deflection responses is described in Section 6.3. It provides a way to determine the corrosion level for those studies which do not give the real corrosion level. Furthermore, it is physically easy for those who carry out tests, compared with the work of extracting the reinforcement from the concrete, cleaning the corrosion product, and measuring the weight of the remaining steel.

6.1 Material properties

6.1.1 Bond-slip model with corrosion effect

The change of bond-slip characteristics with corrosion effects is calculated using the following Eqs. (8)–(14) provided by Feng et al. (2016). The accuracy of this material bond-slip model has been verified by at least 21 data sets of pull-out test including 371 data points and comparison with other four bond-slip models also quantifying the corrosion effect. However, this model (Feng et al., 2016) can be replaced by other bond-slip models including corrosion effect for better fitting. The bond-slip relationship is divided into two parts as mentioned in Section 2: the non-linear ascending branch and the linear descending branch. For the ascending branch, the bond stress τ is expressed by Eq. (8) which is the same as the shape suggested by the FIB model code (FIB, 2013):

$$\tau=\tau_{\max}\left(\frac{\delta}{\delta_1}\right)^{0.4}, \tag{8}$$

where $\tau_{\max}$ is expressed by Eq. (1) in which $\tau_{\max 0}$ is calculated based on the FIB model code (FIB, 2013) and k_τ is expressed differently according to different corrosion levels.

For cor<cor$_{1\text{-}2}$,

$$k_\tau=\left(-0.032\frac{c}{d}+0.576\right)\mathrm{cor}+1, \tag{9}$$

where d is the diameter of reinforcement.

For cor$_{1\text{-}2}\le$ cor$\le$cor$_{2\text{-}3}$,

$$k_\tau=\left(0.0137\frac{c}{d}-0.247\right)\mathrm{cor}+1.42+0.0475\frac{c}{d}-3.94\times10^{-3}\left(\frac{c}{d}\right)^2. \tag{10}$$

For cor>cor$_{2\text{-}3}$,

$$k_\tau=-0.0016\mathrm{cor}+0.224. \tag{11}$$

Moreover, cor$_{1\text{-}2}$ and cor$_{2\text{-}3}$ are expressed by

$$\mathrm{cor}_{1-2}=0.288\frac{c}{d}+1.72, \tag{12}$$

$$\mathrm{cor}_{2-3}=\frac{-1.20-0.0475\frac{c}{d}+3.94\times10^{-3}\left(\frac{c}{d}\right)^2}{0.0137\frac{c}{d}-0.245}. \tag{13}$$

For the descending branch, the bond stress τ can be expressed by

$$\tau=-0.0161\tau_{\max 0}\delta+0.0282\tau_{\max 0}+\tau_{\max}. \tag{14}$$

6.1.2 Material model

Because some parameters were not provided in the literature (Lee et al., 1998; Mangat and Elgarf, 1999; Dekoster et al., 2003), the material model depicted in Eqs. (15) and (16) is considered here. It can be changed or corrected by other models to get more accurate fitting. A linear stress-strain relationship is assumed for the tensile region of concrete while Eq. (15) (Hognestad et al., 1955) is used to determine the concrete stress σ in the compressive region of concrete:

$$\sigma=f_c\left[\frac{2\varepsilon_c}{\varepsilon_{pk}}-\left(\frac{\varepsilon_c}{\varepsilon_{pk}}\right)^2\right], \tag{15}$$

where ε_c is the concrete strain for a concrete stress, ε_{pk} is the concrete strain corresponding to the concrete compressive strength f_c. The definition of ε_{pk} was suggested by Tasdemir et al. (1998) as

$$\varepsilon_{pk}=(-0.067f_c+29.9f_c+1053)\times10^{-6}. \tag{16}$$

6.2 Case 1

Lee et al. (1998) provided results from flexural beam tests with non-corroded and corroded reinforcement. The corrosion level measured as percent mass loss is 3.8%. The material and dimensional properties of the beam which were then summarized by Dekoster et al. (2003) were described as follows. The effective length of the beam L_e is 2000 mm in Fig. 11a. The distance from the loading point to the support is 750 mm and is denoted by a in Fig. 11a. The cross-sectional dimension is 200 mm×250 mm corresponding to b and h shown in Fig. 11b with two tensile reinforcing bars of diameter 13 mm. The cover of the reinforcement is 30 mm. This is the distance from the bottom edge of the concrete to the center of the reinforcement. The compressive strength of concrete f_c is 70.1 MPa. Young's modulus of concrete E_c is 3.85×10^4 MPa. The tensile strength of concrete f_t is 3.67 MPa. The yielding strength of reinforcement f_y is 359.4 MPa. Young's modulus of reinforcement before yielding E_s is 1.97×10^5 MPa.

For a certain load, the deflection in the mid-span point is obtained by the procedures described in Fig. 10. Then the load-deflection response is derived from repeating those procedures with increasing load values. The load capacity can be obtained from the load-deflection curves. The results in Fig. 12a refer to the beam when there is no corrosion in reinforcement while in Fig. 12b the reinforcing bars are corroded to 3.8%. The curve fittings in Fig. 12 show a good

correlation between test results and the results from a segmental approach. The bond-slip model provided by Feng et al. (2016) can also be used to predict the interaction between reinforcement and concrete with corrosion effects.

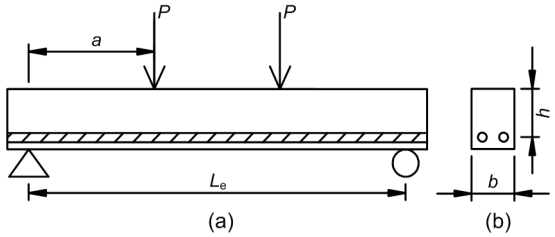

Fig. 11 Dimension properties of the beam
(a) Beam; (b) Cross-section

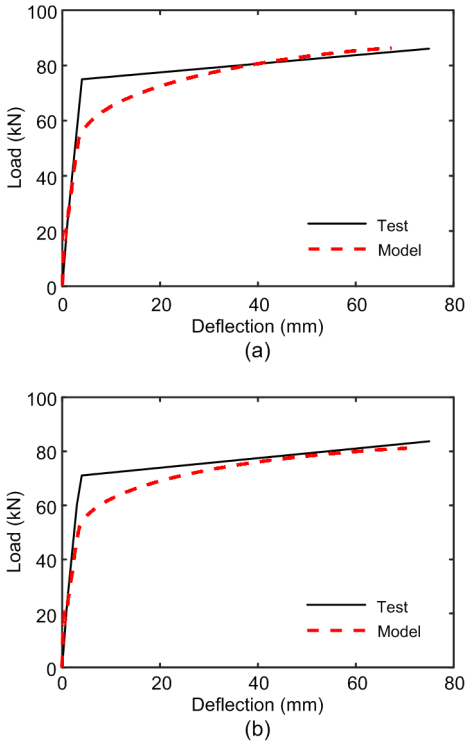

Fig. 12 Comparison of load-deflection curves from M/θ approach and tests
(a) cor=0; (b) cor=3.8%

6.3 Case 2

Flexural testing was carried out by Mangat and Elgarf (1999) with the specimens under four-point loading to get the load-deflection responses as shown in Fig. 11. The whole length of the beams tested by Mangat and Elgarf (1999) is 910 mm and the effective length L_e is 860 mm. The loading point is located at one-third of the beam. The cross-sectional dimension is 100 mm×150 mm. Two tensile reinforcing bars are embedded in the tensile region of the concrete with the concrete cover of 25 mm. The compressive strength of concrete cubes f_c after 28 d is 40 MPa. The yielding strength of reinforcement f_y is 520 MPa. The modulus of elasticity E_s is 2.06×10^5 MPa.

For non-corroded specimens, the load-deflection curves can be obtained directly from the M/θ analysis without deteriorating the bond-slip characteristics of reinforcement. Fig. 13 presents the comparison between the load-deflection curves from the M/θ approach and those provided from tests. It shows that the theoretical results fit well with the test results.

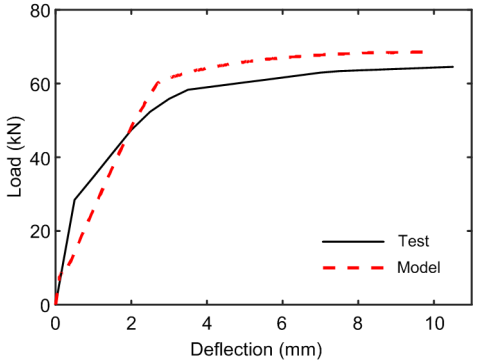

Fig. 13 Load-deflection curves for non-corroded specimens

The specimens tested by Mangat and Elgarf (1999) were reported to be corroded based on a calculation combining loss in bar diameter, years of corrosion, and corrosion current density during test and can be expressed by

$$\mathrm{cor_d}=\frac{2RT}{D}\times100\%, \tag{17}$$

where R is the corrosion rate, T is the years of corrosion, $2RT$ represents the loss of bar diameter, and D is the original diameter of the reinforcing bar. The corrosion levels $\mathrm{cor_d}$ for the specimens are listed in column 1 of Table 1.

This is different from most of the corrosion tests of reinforced concrete in which the corrosion level is calculated as percent mass loss of reinforcement by extracting the reinforcement embedded in the concrete after the flexural tests to measure the real mass

Table 1 Corrosion levels and evaluation of coefficient *e*

cor_d (%)	cor (%)	R=1 mA/cm^2		R=2 mA/cm^2		R=3 mA/cm^2		R=4 mA/cm^2	
		e	cor_{real} (%)	e	cor_{real} (%)	e	cor_{real} (%)	e	cor_{real} (%)
0.00	0.00	3	0.00	3.5	0.00	3.75	0.00	4	0.00
1.25	2.48	3	7.45	3.5	8.70	3.75	9.32	4	9.94
2.50	4.94	3	14.81	3.5	17.28	3.75	18.52	4	19.75
3.75	7.36	3	22.08	3.5	25.76	3.75	27.60	4	29.44
5.00	9.75	3	29.25	3.5	34.13	3.75	36.56	4	39.00
7.50	14.44	3	43.31	3.5	50.53	3.75	54.14	4	57.75
10.00	19.00	3	57.00	3.5	66.50	3.75	71.25	4	76.00

loss (Al-Sulaimani et al., 1990; Almusallam et al., 1996a; Jin and Zhao, 2001; Fang et al., 2004, 2006). Hence, besides the theoretical corrosion levels, the accurate corrosion levels were also provided in those references. However, by the way of the calculation of Mangat and Elgarf (1999), only the theoretical corrosion levels defined in Eq. (17) were given while the actual corrosion levels were not available and could not be measured due to its definition. The following analysis shows how to determine the real corrosion level in tests when only theoretical corrosion levels of reinforcement are provided.

For the corrosion level defined as percent mass loss which is denoted by cor in this paper, from the reduction of the bar diameter $2RT/D$, it can be expressed as

$$\mathrm{cor}=\left(1-\left(1-\frac{2RT}{D}\right)^2\right)\times 100\%. \tag{18}$$

Substituting Eq. (17) into Eq. (18), the relationship between cor as percent mass loss and cor_d defined by Mangat and Elgarf (1999) is calculated by

$$\mathrm{cor}=2\mathrm{cor}_\mathrm{d}-\mathrm{cor}_\mathrm{d}^2. \tag{19}$$

At this stage, the theoretical corrosion levels of the beams (cor) are obtained and listed in column 2 of Table 1. The real corrosion levels denoted by cor_{real} as a function of the theoretical corrosion level cor are expressed as

$$\mathrm{cor}_{\mathrm{real}}=e\times\mathrm{cor}, \tag{20}$$

where the coefficient e is induced to evaluate the relationship between the real corrosion level of reinforcement cor_{real} and the theoretical corrosion level cor. Both cor_{real} and cor are defined as percent weight loss of the original reinforcement. For a constant cor_d equal to 7.50%, the load-deflection curves are different corresponding to different corrosion rates as shown in Figs. 14a–14d. Different values of the coefficient e are used to find the real corrosion level cor_{real} to make the load-deflection curves fit well with the test results. This is a procedure of trial and error. The results of the coefficient e for corrosion rates of 1 mA/cm^2, 2 mA/cm^2, 3 mA/cm^2, and 4 mA/cm^2 are listed in columns 3, 5, 7, and 9 of Table 1, respectively. When cor_d is fixed at 7.50%, the comparison between test results and the results from M/θ approach based on the corrosion level corrected by coefficient e is shown in Fig. 14. It implies that the guesses of coefficient e for different corrosion rates when cor_d remains at 7.50% are such that the numerical results fit well with the test results.

Now let us see whether the guesses of coefficient e are such that the load-deflection curves from numerical approach fit with test results when the corrosion rate is constant but cor_d is changing. Fig. 15 shows the load-deflection responses referring to the corrosion rate of 4 mA/cm^2 compared with the curves from the presented approach with the coefficient e of 4. In addition, Fig. 16 (p.291) shows the load-deflection responses with corrosion rate equal to 2 mA/cm^2 compared with the curves of the corrosion levels corrected by e equal to 3.5. The comparisons in Figs. 15 and 16 show a good correlation between numerical and test results. This indicates that the guesses of coefficient e are correct and the corrosion levels corrected by coefficient e are very close to the real corrosion levels. Hence, the evaluated corrosion levels listed in columns 4, 6, 8, and 10 in Table 1 can be taken as the real corrosion levels for the reinforcement embedded in specimens.

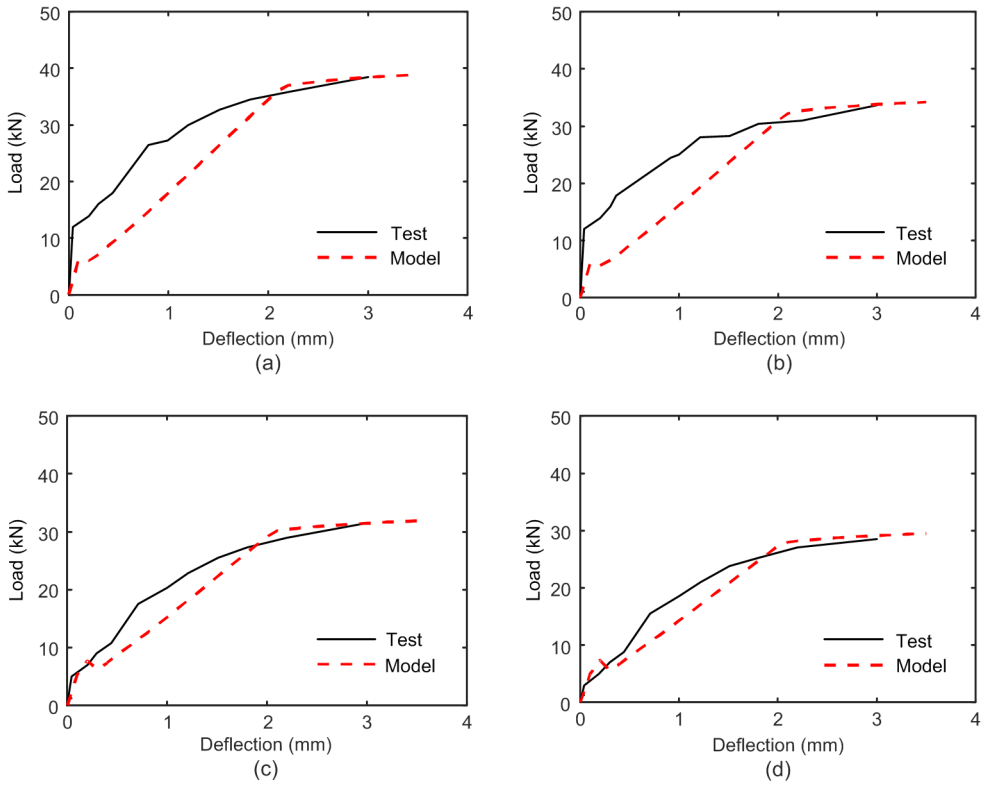

Fig. 14 Load-deflection curves for cor_d=7.50% with different corrosion rates
(a) R=1 mA/cm^2, e=3; (b) R=2 mA/cm^2, e=3.5; (c) R=3 mA/cm^2, e=3.75; (d) R=4 mA/cm^2, e=4

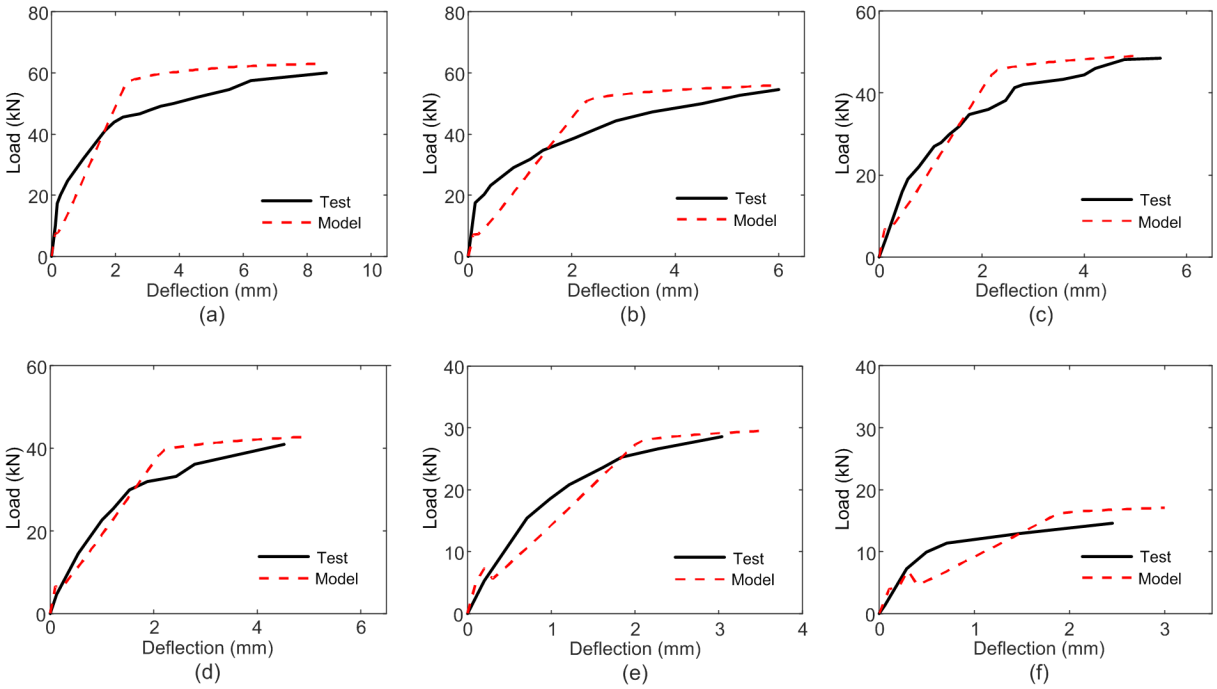

Fig. 15 Load-deflection curves fitting for corrosion rate equal to 4 mA/cm^2
(a) cor_d=1.25%; (b) cor_d=2.50%; (c) cor_d=3.75%; (d) cor_d=5.00%; (e) cor_d=7.50%; (f) cor_d=10.00%

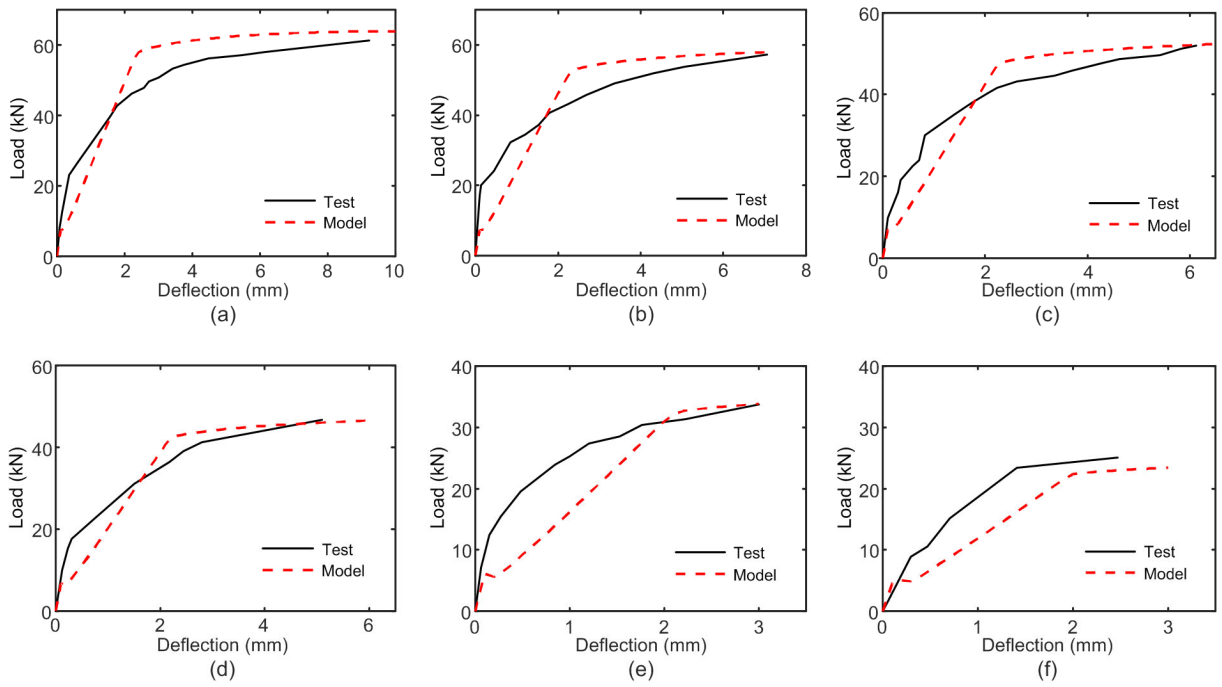

Fig. 16 Load-deflection curves fitting for corrosion rate equal to 2 mA/cm^2
(a) cor_d=1.25%; (b) cor_d=2.50%; (c) cor_d=3.75%; (d) cor_d=5.00%; (e) cor_d=7.50%; (f) cor_d=10.00%

7 Conclusions

A numerical partial-interaction moment-rotation (M/θ) approach is proposed in this study to simulate the corrosion effects on the short-term behavior of reinforced concrete beams. The presented M/θ approach allows for tension-stiffening analysis by adopting bond-slip characteristics between reinforcement and adjacent concrete in partial-interaction analysis.

The moment-curvature (M/χ) relationship is derived from the M/θ analysis and is adopted to obtain the deflection distribution along the beam. Then the load-deflection responses are obtained through standard analytical techniques. The bond-slip model with corrosion effect provides guidance on how to change the bond-slip characteristics due to certain corrosion levels and material properties. Furthermore, the deterioration of bond-slip characteristics reflects the corrosion effect on the load-deflection responses. A good agreement is shown between the numerical load-deflection curves and the flexural test results.

The numerical M/θ method along with the bond-slip model with corrosion effect is also used to predict the real corrosion levels of reinforcement. The procedure of trial and error is described by combining an example in which the actual corrosion levels are not given beside the theoretical corrosion levels.

8 Outlook

The presented numerical technique could be extended to quantify the confinement effect on structural behavior of reinforced concrete just by changing the bond-slip characteristics into those with confinement effects. Additionally, the time effect on the development of crack width or deflection could be analyzed by adding shrinkage, creep, or temperature into the model as well as the corrosion effect.

Contributors

Qian FENG and Rong-qiao XU designed the research. Qian FENG and Yong-ping ZHANG processed the corresponding data. Qian FENG wrote the first draft of the manuscript. Guan-nan WANG and Rong-qiao XU helped to organize the manuscript. Qian FENG and Rong-qiao XU revised and edited the final version.

Conflict of interest

Qian FENG, Guan-nan WANG, Yong-ping ZHANG, and Rong-qiao XU declare that they have no conflict of interest.

References

Almusallam AA, Al-Gahtani AS, Aziz AR, et al., 1996a. Effect of reinforcement corrosion on bond strength. *Construction and Building Materials*, 10(2):123-129. https://doi.org/10.1016/0950-0618(95)00077-1

Almusallam AA, Al-Gahtani AS, Aziz AR, et al., 1996b. Effect of reinforcement corrosion on flexural behavior of concrete slabs. *Journal of Materials in Civil Engineering*, 8(3):123-127. https://doi.org/10.1061/(asce)0899-1561(1996)8:3(123)

Al-Sulaimani GJ, Kaleemullah M, Basunbul IA, et al., 1990. Influence of corrosion and cracking on bond behavior and strength of reinforced concrete members. *ACI Structural Journal*, 87(2):220-231.

Branson DE, 1977. Deformation of Concrete Structures. McGraw-Hill, New York, USA.

Cabrera JG, 1996. Deterioration of concrete due to reinforcement steel corrosion. *Cement and Concrete Composites*, 18(1):47-59. https://doi.org/10.1016/0958-9465(95)00043-7

Chapman RA, Shah SP, 1987. Early-age bond strength in reinforced concrete. *ACI Materials Journal*, 84(6):501-510.

Dekoster M, Buyle-Bodin F, Maurel O, et al., 2003. Modelling of the flexural behaviour of RC beams subjected to localised and uniform corrosion. *Engineering Structures*, 25(10):1333-1341. https://doi.org/10.1016/S0141-0296(03)00108-1

Fang CQ, Lundgren K, Chen LG, et al., 2004. Corrosion influence on bond in reinforced concrete. *Cement and Concrete Research*, 34(11):2159-2167. https://doi.org/10.1016/j.cemconres.2004.04.006

Fang CQ, Lundgren K, Plos M, et al., 2006. Bond behaviour of corroded reinforcing steel bars in concrete. *Cement and Concrete Research*, 36(10):1931-1938. https://doi.org/10.1016/j.cemconres.2006.05.008

Feng Q, Visintin P, Oehlers DJ, 2016. Deterioration of bond–slip due to corrosion of steel reinforcement in reinforced concrete. *Magazine of Concrete Research*, 68(15):768-781. https://doi.org/10.1680/jmacr.15.00217

Feng Q, Visintin P, Oehlers DJ, 2018. Effect of steel bar corrosion on flexural behaviour through bond. *Proceedings of the Institution of Civil Engineers–Structures and Buildings*, 171(5):380-394. https://doi.org/10.1680/jstbu.16.00168

FIB, 2013. FIB Model Code for Concrete Structures 2010. Ernst & Sohn, Berlin, Germany. https://doi.org/10.1002/9783433604090

Fu X, Chung DDL, 1997. Effect of corrosion on the bond between concrete and steel rebar. *Cement and Concrete Research*, 27(12):1811-1815. https://doi.org/10.1016/S0008-8846(97)00172-5

Gilbert RI, Mickleborough NC, 1990. Design of Prestressed Concrete. Unwin Hyman Ltd., London, UK.

Haskett M, Oehlers DJ, Ali MSM, 2008. Local and global bond characteristics of steel reinforcing bars. *Engineering Structures*, 30(2):376-383. https://doi.org/10.1016/j.engstruct.2007.04.007

Haskett M, Oehlers DJ, Ali MSM, et al., 2009. Rigid body moment–rotation mechanism for reinforced concrete beam hinges. *Engineering Structures*, 31(5):1032-1041. https://doi.org/10.1016/j.engstruct.2008.12.016

Hognestad E, Hanson NW, McHenry D, 1955. Concrete stress distribution in ultimate strength design. *Journal Proceedings*, 52(12):455-480.

Jiang C, Wu YF, Dai MJ, 2018. Degradation of steel-to-concrete bond due to corrosion. *Construction and Building Materials*, 158:1073-1080. https://doi.org/10.1016/j.conbuildmat.2017.09.142

Jin WL, Zhao YX, 2001. Effect of corrosion on bond behavior and bending strength of reinforced concrete beams. *Journal of Zhejiang University-SCIENCE*, 2(3):298-308. https://doi.org/10.1631/jzus.2001.0298

Johnston B, Cox KC, 1940. The bond strength of rusted deformed bars. *Journal Proceedings*, 37:57-72.

Knight D, Visintin P, Oehlers DJ, et al., 2013. Incorporating residual strains in the flexural rigidity of RC members with varying degrees of prestress and cracking. *Advances in Structural Engineering*, 16(10):1701-1718. https://doi.org/10.1260/1369-4332.16.10.1701

Knight D, Visintin P, Oehlers DJ, et al., 2014. Short-term partial-interaction behavior of RC beams with prestressed FRP and steel. *Journal of Composites for Construction*, 18(1):04013029. https://doi.org/10.1061/(ASCE)CC.1943-5614.0000408

Knight D, Visintin P, Oehlers DJ, 2015. Displacement-based simulation of time-dependent behaviour of RC beams with prestressed FRP or steel tendons. *Structural Concrete*, 16(3):406-417. https://doi.org/10.1002/suco.201400039

Lee HS, Noguchi T, Tomosawa F, 1998. Fundamental study on evaluation of structural performance of reinforced concrete beam damaged by corrosion of longitudinal tensile main rebar by finite element method. *Journal of Structural and Construction Engineering*, 506:43-50.

Lee HS, Noguchi T, Tomosawa F, 2002. Evaluation of the bond properties between concrete and reinforcement as a function of the degree of reinforcement corrosion. *Cement and Concrete Research*, 32(8):1313-1318. https://doi.org/10.1016/S0008-8846(02)00783-4

Lin HW, Zhao YX, Feng P, et al., 2019. State-of-the-art review on the bond properties of corroded reinforcing steel bar. *Construction and Building Materials*, 213:216-233. https://doi.org/10.1016/j.conbuildmat.2019.04.077

Lundgren K, 2002. Modelling the effect of corrosion on bond in reinforced concrete. *Magazine of Concrete Research*, 54(3):165-173. https://doi.org/10.1680/macr.2002.54.3.165

Mangat PS, Elgarf MS, 1999. Flexural strength of concrete beams with corroding reinforcement. *Structural Journal*, 96(1):149-158.

Muhamad R, Ali MSM, Oehlers DJ, et al., 2011. Load-slip relationship of tension reinforcement in reinforced concrete members. *Engineering Structures*, 33(4):1098-1106. https://doi.org/10.1016/j.engstruct.2010.12.022

Muhamad R, Ali MSM, Oehlers DJ, et al., 2012. The tension stiffening mechanism in reinforced concrete prisms. *Advances in Structural Engineering*, 15(12):2053-2069. https://doi.org/10.1260/1369-4332.15.12.2053

Nawy EG, 2006. Prestressed Concrete: a Fundamental Approach, 5th Edition. Prentice Hall, Upper Saddle River, USA.

Oehlers DJ, Liu IST, Seracino R, 2005. The gradual formation of hinges throughout reinforced concrete beams. *Mechanics Based Design of Structures and Machines*, 33(3-4):373-398. https://doi.org/10.1080/15367730500458234

Oehlers DJ, Ali MSM, Haskett M, et al., 2011. FRP-reinforced concrete beams: unified approach based on IC theory. *Journal of Composites for Construction*, 15(3):293-303. https://doi.org/10.1061/(ASCE)CC.1943-5614.0000173

Oehlers DJ, Muhamad R, Ali MSM, 2013. Serviceability flexural ductility of FRP RC beams: a discrete rotation approach. *Construction and Building Materials*, 49:974-984. https://doi.org/10.1016/j.conbuildmat.2012.10.001

Peattie KR, Pope JA, 1956. Effect of age of concrete on bond resistance. *Journal Proceedings*, 52(2):661-672.

Tasdemir MA, Tasdemir C, Akyüz S, et al., 1998. Evaluation of strains at peak stresses in concrete: a three-phase composite model approach. *Cement and Concrete Composites*, 20(4):301-318. https://doi.org/10.1016/S0958-9465(98)00012-2

Thompson KJ, Park R, 1980. Ductility of prestressed and partially prestressed concrete beam sections. *PCI Journal*, 25(2):46-70. https://doi.org/10.15554/pcij.03011980.46.70

Tondolo F, 2015. Bond behaviour with reinforcement corrosion. *Construction and Building Materials*, 93:926-932. https://doi.org/10.1016/j.conbuildmat.2015.05.067

Visintin P, Oehlers DJ, Wu C, et al., 2012. A mechanics solution for hinges in RC beams with multiple cracks. *Engineering Structures*, 36:61-69. https://doi.org/10.1016/j.engstruct.2011.11.028

Visintin P, Oehlers DJ, Muhamad R, et al., 2013a. Partial-interaction short term serviceability deflection of RC beams. *Engineering Structures*, 56:993-1006. https://doi.org/10.1016/j.engstruct.2013.06.021

Visintin P, Oehlers DJ, Haskett M, 2013b. Partial-interaction time dependent behaviour of reinforced concrete beams. *Engineering Structures*, 49:408-420. https://doi.org/10.1016/j.engstruct.2012.11.025

Visintin P, Sturm AB, Oehlers DJ, 2018. Long- and short-term serviceability behavior of reinforced concrete beams: mechanics models for deflections and crack widths. *Structural Concrete*, 19(2):489-507. https://doi.org/10.1002/suco.201700022

Warner RF, Rangan BV, Hall AS, et al., 1998. Concrete Structures. Longman, Melbourne, Australia.

Yalciner H, Eren O, Sensoy S, 2012. An experimental study on the bond strength between reinforcement bars and concrete as a function of concrete cover, strength and corrosion level. *Cement and Concrete Research*, 42(5):643-655. https://doi.org/10.1016/j.cemconres.2012.01.003

中文概要

题　目：基于分段法的锈蚀钢筋混凝土梁荷载-挠度特性数值模拟和钢筋锈蚀程度评估

目　的：探讨在钢筋开始锈蚀后的混凝土梁荷载-挠度特性的变化，并利用荷载-挠度曲线反推钢筋锈蚀程度，进而为预测锈蚀钢筋混凝土结构行为提供新的依据。

创新点：1. 通过模拟钢筋混凝土的粘结滑移，建立计算荷载-挠度特性的数值方法。2. 利用新建立的方法，评估结构内部钢筋锈蚀程度。

方　法：1. 通过模拟钢筋与混凝土之间的粘结滑移作用，得到端部滑移量对应的作用于钢筋上的荷载值。2. 将滑移量-荷载值关系导入钢筋混凝土梁的荷载-挠度曲线模型中，对受拉区混凝土开裂前后的钢筋混凝土梁的荷载-挠度曲线关系进行模拟。3. 在不同钢筋锈蚀程度下对已知荷载-挠度关系曲线的钢筋混凝土梁进行荷载-挠度曲线计算，拟合出相似的荷载-挠度曲线，进而预测结构内部的钢筋锈蚀程度。

结　论：1. 随着钢筋锈蚀程度的不断增加，钢筋混凝土梁的承载力明显下降。2. 钢筋与混凝土的粘结滑移可以模拟钢筋锈蚀加剧后的挠度发展变化。3. 利用新建立的数值方法可以有效地预测结构内部的钢筋锈蚀程度。

关键词：钢筋混凝土；锈蚀；荷载-挠度；受拉强化；粘结滑移